Coastal Engineering 57 (2010) 30–40

Contents lists available at ScienceDirect

Coastal Engineering

journal homepage: www.elsevier.com/locate/coastaleng

The form of the asymptotic depth-limited wind-wave spectrum Part III — Directional spreading

I.R. Young

Faculty of Engineering and Industrial Sciences, Swinburne University of Technology, P.O. Box 218, Hawthorn, Vic 3122, Melbourne, Australia

ARTICLE INFO

Article history:
Received 23 May 2009
Received in revised form 31 August 2009
Accepted 3 September 2009
Available online 9 October 2009

Keywords:
Wind generated waves
Finite depth
Wave spectrum
Wavenumber spectrum
Wavelet directional method (WDM)

ABSTRACT

The directional spreading of both the wavenumber and frequency spectra of finite-depth wind generated waves at the asymptotic depth limit are examined. The analysis uses the Wavelet Directional Method, removing the need to assume a form for the dispersion relationship. The paper shows that both the wavenumber and frequency forms are narrowest at the spectral peak and broaden at wavenumbers (frequencies) both above and below the peak. The directional spreading of the wavenumber spectrum is bi-modal above the spectral peak. In contrast, the frequency spectrum is uni-modal. This difference is shown to be the result of energy in the wind direction being displaced from the linear dispersion shell. A full parametric relationship for the directional spreading of the wavenumber spectrum is developed. The analysis clearly shows that typical dispersion relationships are questionable at high frequencies and that such effects can be significant. This result supports greater attention being focussed on the routine recording of wavenumber spectra, rather than frequency spectra.

1. Introduction

The asymptotic depth-limited spectrum is the limiting form which results when a constant wind blows over a large body of uniformly finite-depth water. The resulting spectrum is hence a balance between atmospheric input, bottom friction, breaking dissipation and various nonlinear processes (3-wave and 4-wave). In essence, this spectral form is the finite-depth analogy of the deep-water asymptote represented by the Pierson–Moskowitz form (Pierson and Moskowitz, 1964). The finite-depth asymptotic form is of importance for a number of reasons. As the asymptotic form, it is the limiting design condition in finite-depth situations and is hence of engineering significance. As, by definition, all source terms (input, dissipation, bottom friction and nonlinear interaction) are in balance, this spectral form provides valuable indirect information on the physics of wind-wave generation in finite-depth conditions. Finally, as will become obvious in this paper, nonlinear processes become important in these situations and hence the spectral form gives insight to the importance of such processes in intermediate-depth conditions.

There are numerous observations of finite-depth spectra reported in the literature. The vast majority of these represent shoaling conditions, where deep-water waves have propagated into areas of finite depth. Observations of locally-generated waves in finite-depth conditions are much rarer. The classic data sets from Lake Okeechobee, USA (Thijsse, 1949; U.S. Army Corps of Engineers, 1955; Bretschneider, 1958) considered the asymptotic limits of integral parameters such as total energy (wave height) and period. The more recent studies have largely considered the data sets taken in the mid 1990s at Lake George, Australia (Young and Verhagen, 1996a,b; Young et al., 1996; Resio et al., 2004). These studies, together with data from Lake Ijssel, The Netherlands (Bottema, 2007; Bottema and van Vledder, 2009) have considered the form of the full frequency spectrum, including some analysis of directional spreading.

This paper is the third in a series which analyses data taken with a high resolution spatial array in Lake George in 1997 and 1998. Young and Babanin (2006) (henceforth called Part I) considered the asymptotic limits for total energy (significant wave height) and peak frequency, as well as developing a parametric form for the one-dimensional frequency spectrum. This result was extended in Young and Babanin (2009) (henceforth called Part II) where they used the Wavelet Directional Method to study the one-dimensional wavenumber spectrum. This paper extends the analysis of Part II to consider the full directional spectrum in both wavenumber and frequency forms.

The arrangement of the paper is as follows. Section 2 provides a brief overview of observations of the directional wave spectrum, with particular reference to finite-depth conditions. Section 3 summarises the present experimental configuration and the data used in the analysis. This is followed in Section 4 by a description of the Wavelet Directional Method (MDM) which is used to analyse the present data set. Initial observations of the directional spreading are made in

E-mail address: iyoung@swin.edu.au.

0378-3839/$ – see front matter © 2009 Elsevier B.V. All rights reserved.
doi:10.1016/j.coastaleng.2009.09.001

Section 5, which is followed by a detailed analysis in Section 6. The results are discussed in detail in Section 7 and conclusions are drawn in Section 8.

2. Observations of the finite-depth directional spectrum

2.1. Directional spreading function

It is common practice to consider the directional frequency spectrum, $E(f, \theta)$ or directional wavenumber spectrum, $F(k, \theta)$, where f is frequency, $k=|\underline{k}|$ is the modulus of the wavenumber vector and θ is direction (Longuet-Higgins et al., 1963) in the form:

$$E(f,\theta) = E(f)D(f,\theta) \tag{1}$$

$$F(k,\theta) = F(k)D(k,\theta) \tag{2}$$

where $E(f)$ is the one-dimensional frequency spectrum, $F(k)$ is the one-dimensional wavenumber spectrum and D is a directional spreading function, defined such that

$$\int_0^{2\pi} D(k,\theta)d\theta = \int_0^{2\pi} D(f,\theta)d\theta = 1 \tag{3}$$

An alternative representation of the spreading function is

$$D(k,\theta) = B(k)K(k,\theta) \tag{4}$$

where $B(k)$ is a normalization factor and K is defined such that it has a maximum value of one at each wavenumber. A similar relationship can be written for the frequency-based spreading function.

For simplicity, the spreading function, K is often represented in a parametric form. Three formulations are commonly used: $K(k)=\cos^{2s(k)}\theta/2$ (Longuet-Higgins et al., 1963), $K(k)=\mathrm{sech}^2\beta(k)\theta$ (Donelan et al., 1985) and $A^{-1}(k) = \int_0^{2\pi} K(k,\theta)d\theta$ (Babanin and Soloviev, 1998). In each case, the width of the spreading function is represented by a single parameter at each wavenumber (i.e. s, β or A). Again, similar relationships can be written for the frequency spectrum.

In deep water, the classical observations of the directional spreading were made by Mitsuyasu et al. (1975), Hasselmann et al. (1980) and Donelan et al. (1985). The Donelan et al. (1985) measurements were made using a spatial array of wave gauges, whilst the other investigations used pitch–roll–heave (3-axis) buoys. The analysis of all data sets assumed spreading functions of the form K described above. The details of the spectral width varied considerably between these experiments. All, however, revealed directional spreading which was narrowest at the frequency of the spectral peak and broadened with frequency both above and below the peak frequency.

Young (1994) investigated the analysis techniques used and showed that the results were sensitive to the chosen technique, which probably explained the differences in the results. In addition, Young (1994) concluded that instruments with a limited number of sensors (e.g. 3-axis) yielded results with artificially broad spectra. This is consistent with the observation that the Donelan et al. (1985) results were narrower than the earlier measurements.

Young et al. (1995) examined spectra obtained from a spatial array of wave gauges, but analysed the results using a Maximum Likelihood Method (MLM) (Isobe et al., 1984) which did not prescribe an *a priori* directional form. Rather than the uni-modal structure previously parameterised by cosine-type forms, they found bi-modal spreading around the mean wind direction. They explained that this structure resulted from 4-wave nonlinear interactions (Hasselmann, 1962; Banner and Young, 1994). Numerical calculations with a full solution to the nonlinear term produced similar bi-modal forms. There was also evidence that such spreading was present in the directional wavenumber spectra observed by Holthuijsen (1983) using stereo-photography.

Following the initial observations of Young et al. (1995), a number of observations of bi-modal spreading have been reported. Wang and Hwang (2001) and Ewans (1998) have reported bi-modal frequency spectra obtained from MLM analysis of buoy data, whereas Wyatt (1995) and Hwang et al. (2000) have reported bi-modal wavenumber spectra obtained from scanning radar measurements.

As explained by Young (1994), some doubt can be raised about such MLM analyses, where there is evidence that the analysis technique can sometimes produce spurious side lobes. However, the reports of bi-modal wavenumber spectra measured by both stereo-photography and scanning radar systems seem compelling. The supporting numerical (theoretical) calculations again support this structure.

The only comprehensive measurements of the directional spreading of locally-generated wind-waves in finite-depth conditions are those of Young et al. (1996). These results showed a form qualitatively similar to deep-water observations with the spreading narrowest at the spectral peak frequency and broadening both above and below the peak. There did not appear to be a systematic dependence on non-dimensional water depth, but the spectra were significantly broader than previous deep-water observations.

2.2. One-dimensional spectrum

Following on from the finite-depth spectral observations of Young and Verhagen (1996b) and Bottema (2007), Parts I and II considered the forms of the one-dimensional frequency and wavenumber spectra at the asymptotic depth-limit, respectively. The frequency spectrum was similar to deep-water observations (eg. Donelan et al., 1985) with the addition of a small harmonic at $2f_p$, where f_p is the frequency of the spectral peak. This form was parameterized as:

$$E(f) = E_1(f) + E_2(f) \tag{5}$$

where

$$E_1(f) = \beta_1 g^2 (2\pi)^{-4} f_{p_1}^{-(5+n_1)} f^{n_1} \exp\left[\frac{n_1}{4}\left(\frac{f}{f_{p_1}}\right)^{-4}\right] \cdot \gamma_1^{\exp\left[\frac{-(f-f_{p_1})^2}{2\sigma_1^2 f_{p_1}^2}\right]} \tag{6}$$

$$E_2(f) = \beta_2 g^2 (2\pi)^{-4} f_{p_2}^{-(5+n_2)} f^{n_2} \exp\left[\frac{n_2}{4}\left(\frac{f}{f_{p_2}}\right)^{-4}\right] \tag{7}$$

and the parameters in Eqs. (6) and (7) can be represented by:

$$\beta_1 = 5.89 \times 10^{-3} \delta^{0.085} \tag{8}$$

$$\gamma_1 = 2.97 \times 10^{-3} \beta_1^{-1.34} \tag{9}$$

$$\sigma_1 = 2.0 \times 10^{-6} \beta_1^{-2.09} \tag{10}$$

and $n_1=-4$, $n_2\approx-8.35$ and $\beta_2\approx0.074$. The parameter δ in Eq. (8) is the non-dimensional water depth, $\delta=gd/U_{10}^2$, where U_{10} is the wind speed measured at a reference height of 10 m and d is the water depth.

In contrast, the wavenumber form was far simpler, being represented by:

$$F(k) = \beta k_p^{-(3+n)} k^n \exp\left[\frac{n}{4}\left(\frac{k}{k_p}\right)^{-3}\right] \tag{11}$$

with

$$\beta = 6 \times 10^{-3} \delta^{-0.2} \tag{12}$$

and $n=-2.8$.

The fact that there is not a one-to-one relationship between the frequency and wavenumber spectra was shown to be a result of nonlinear processes in the finite-depth conditions which resulted in wave energy being bound to the spectral peak and not conforming to a traditional linear dispersion relationship. The bound harmonic at $2f_p$ in the frequency spectrum is a clear example of such behaviour.

3. Experimental setup and available data

Wave data were collected in Lake George in south-eastern Australia. This site has been well documented in the previous studies of Young and Verhagen (1996a,b) and Young et al. (1996). The measurements were made from a platform on the eastern shore of the lake. This experimental site and the instrumentation and data recorded for this experiment have been reported in detail in Young et al. (2005), Part I and Part II. A broad range of environmental parameters were recorded as part of the full experimental program. Of particular relevance to this study, coincident measurements of the water surface elevation, water depth and wind speed at a reference height of 10 m were made. The water surface elevation measurements were made using a spatial array in the form of a centred pentagon of radius 15 cm. The details of the instrumentation are described in Part II. The probes in the array were coincidently sampled at 25 Hz, records consisting of 20 min duration (i.e. 30,000 samples per probe).

The array data was analysed using the Wavelet Directional Method (WDM) (see Section 4) to obtain wavenumber spectra. The wave probe records were sub-divided into blocks of 256 points and the wavelets formed using an analysis with 8 voices. The wavelet analysis considers the wave field to be made up of a summation of independent Morlet wavelets, each of different scale [Donelan et al., 1996]. To improve accuracy, it is common to carry out the analysis at additional intermediate scales, called voices. The number of voices was varied between 4 and 12 with little impact on the resulting spectra. Part I presented a detailed analysis of the confidence limits associated with the resulting Fourier spectra. Such an analysis is beyond the scope of this paper, as the statistical variability of WDM derived spectra is yet to be determined. However, 6 times as much data is used to derive each spectrum in the WDM analysis compared to the Fourier analysis of Part I. Therefore, it is reasonable to assume that the confidence limits will not be larger than those for Part I (i.e. the upper and lower 95% confidence limits are given by $1.3F(k)$ and $0.8F(k)$, respectively, where $F(k)$ is the estimate of the spectral ordinate).

The full data set is summarised in Table 1 of Part I. The wind speed range spans $5.6\ \mathrm{m/s} < U_{10} < 19.8\ \mathrm{m/s}$ and water depths are in the range $0.6\ \mathrm{m} < d < 1.15\ \mathrm{m}$ and non-dimensional depth, $k_p d$ in the range $0.71 < k_p d < 3.5$. Noting that deep-water conditions are usually assumed for $k_p d > \pi$ and shallow water conditions for $k_p d < \pi/10$, the present data set spans most of the transitional water depth region.

All other details of the experimental configuration and sampling can be found in Part I and Part II.

4. The wavelet directional method

The most obvious way to measure the directional wavenumber spectrum, $F(\underline{k})$, where $\underline{k}$ is the two-dimensional wavenumber vector is to digitize the two-dimensional spatial domain (x, y). This can be done by stereo-photography (Holthuijsen, 1983; Banner et al., 1989) or indirectly through a remote-sensing technique (e.g. Alpers et al., 1981; Young et al., 1985; Hasselmann et al., 1985; Walsh et al., 1989). These approaches have either logistical difficulties (stereo-photography) or rely on still incomplete knowledge of transfer functions (remote-sensing).

The standard approaches to the analysis of spatial array data (as in the present experiment) consist of the Fourier expansion method (Longuet-Higgins et al., 1963), the Maximum Likelihood Method (MLM) (Isobe et al., 1984) or the Maximum Entropy Method (MEM) (Lygre and Krogstad, 1986). These methods all assume a linear Fourier representation of the water surface. As the spatial array has too few degrees of freedom to define the two-dimensional surface elevation, an approximate form is developed which either conforms to a pre-determined parametric shape or maximizes the likelihood or entropy of the solution. In contrast, the Wavelet Directional Method (WDM) (Donelan et al., 1996; Krogstad et al., 2006) makes two assumptions: that the water surface can be represented by a summation of Morlet wavelets and that only one such wavelet is within the footprint of the array at any instant. Both of these assumptions seem reasonable. It is well known that Fourier expansions can represent complex water surfaces accurately. As wavelets provide greater flexibility, then we can be confident that a good approximation to the water surface can be found. Details of the mathematical form of the Morlet wavelet can be found in Donelan et al. (1996). In physical space, however, a Morlet wavelet looks like a wave group or packet of energy. In contrast to a sinusoidal form (Fourier analysis) it has a finite spatial extent. Thus, the wavelet analysis can be considered as representing the water surface by a summation of wave packets, rather than a summation of stationary sinusoidal forms. The summation runs over wavelets with different spatial extent and frequency, with no requirement for a unique dispersion relationship linking these parameters. As a result, the wavelet approach is very flexible when considering non-homogeneous data or data where the dispersion relationship between wavenumber and frequency is unknown.

Typical wavelets used in the analysis will have a spatial extent of tens of metres. As the footprint of the array is much smaller (an order of magnitude) than such wavelets, it is reasonable to assume that for the vast bulk of the time, only one wavelet will be within the array at any instant. Hence, this criterion is generally satisfied.

With these assumptions, the wavenumber vector can be determined by considering the phase difference of the wavelet between the gauges of the array. The phase difference between the gauges i and j is given by (Donelan et al., 1996; Krogstad et al., 2006; Part II)

$$\phi_{ij}(t) = k_x(t)X_{ij} + k_y(t)Y_{ij} \tag{13}$$

where (X_{ij}, Y_{ij}) denotes the spatial separation vector between a pair of gauges defined by the geometry of the array and (k_x, k_y) are the orthogonal components of the wavenumber vector $\underline{k}$. Eq. (13) has two unknowns, k_x and k_y and hence provided there are more than two elements in the array it can be solved to uniquely determine the wavenumber vector. The resulting solution yields a series of n wavelets, each with an amplitude $AA(f, n)$, direction $dd(f, n)$ and wavenumber modulus $kk(f, n)$. Thus by summing the squares of the amplitudes of the wavelets (AA^2) it is possible to form: the directional frequency spectrum, the directional wavenumber spectrum, the frequency–wavenumber spectrum, $\Psi(k, f)$ (i.e. dispersion relation) and the dispersion relation as a function of direction, $\Psi(k, f, \theta)$. Note that in this analysis no *a priori* dispersion relationship is required. Rather, this is an element of the solution.

A more detailed explanation of the WDM is provided in Part II. The description above reveals an analysis technique ideally suited to investigate the directional spreading of nonlinear waves.

5. Observations of the directional spreading function

As outlined in Parts I and II, the data considered in this paper were recorded over a period of approximately 1 year from September 1997 to October 1998. A total of 55 records were analysed using the WDM. All of these records could be classified as intermediate water depth ($k_p d$ between 0.7 and 1.99) with approximately half at the asymptotic limit to growth defined in Part I.

Fig. 1 shows a typical example of the resulting directional spectra. The case shown is for c061323.oc8, as defined in Part II ($H_s = 0.336$m,

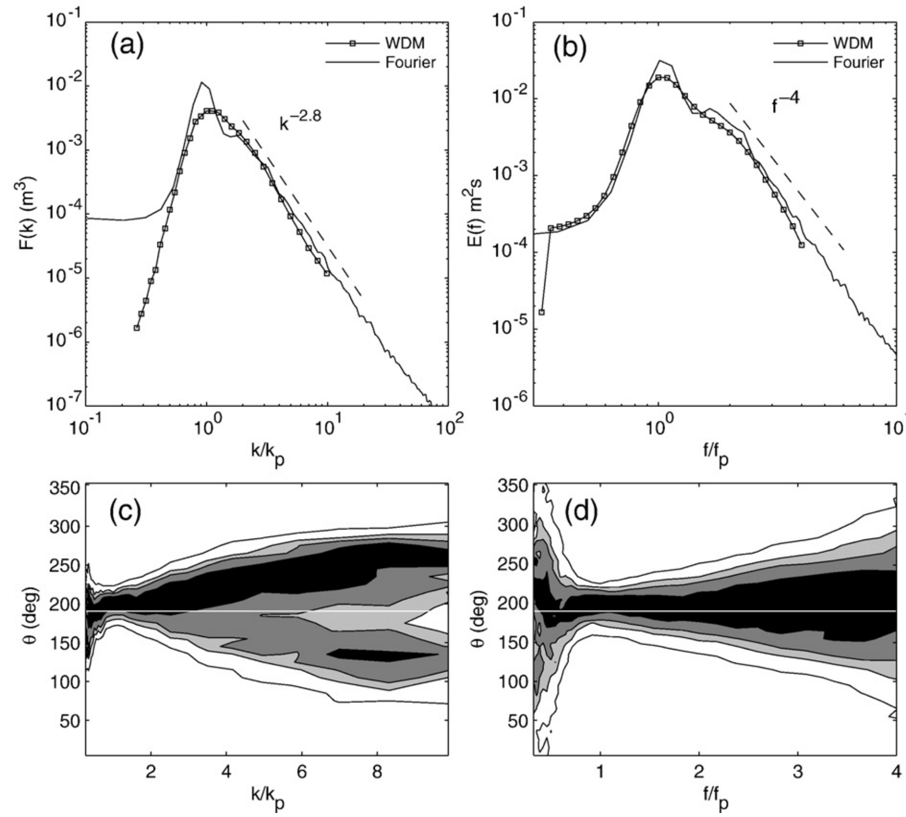

Fig. 1. The directional wavenumber spectrum, $F(k, \theta)$and the directional frequency spectrum, $E(f, \theta)$ for case c061323,oc8 (see Part II). Panel (a) shows the one-dimensional wavenumber spectrum derived from the WDM analysis (solid line with squares) and derived from a conventional Fourier analysis (solid line). The dashed line is a reference $k^{-2.8}$ slope. Panel (b) shows the one-dimensional frequency spectrum (definitions as in Panel (a)). The dashed line is a reference f^{-4} slope. Panels (c) and (d) show the spreading functions $K(k, \theta)$ and $K(f, \theta)$, respectively. By definition this spreading function has a maximum value of 1.0 at each wavenumber (or frequency). Contours are drawn at 0.70, 0.40, 0.25, and 0.10. The horizontal white line is the mean wind direction.

$f_p = 0.406$Hz, $U_{10} = 13.3$m/s, $d = 0.97$ m). Fig. 1 shows the one-dimensional wavenumber spectrum, $F(k)$ (Fig. 1a) and the one-dimensional frequency spectrum, $E(f)$ (Fig. 1b). In each case the WDM analysis is shown, together with a standard Fourier analysis. In the case of $F(k)$, the Fourier form has been derived from the corresponding frequency spectrum, assuming the linear dispersion relationship [$\omega^2 = gk\tanh(kd)$, where $\omega = 2\pi f$]. As reported in Parts I and II, the frequency spectrum has a high frequency face proportional to f^{-4}, with a small harmonic visible at approximately $2f_p$. The wavenumber spectrum has a high wavenumber face proportional to $k^{-2.8}$. No harmonic is present and the general form is simpler than the frequency spectrum [see Eqs. (5) and (11)].

Fig. 1c shows the corresponding directional spreading function, $K(k)$ and Fig. 1d, the frequency form, $K(f)$. Note that at each wavenumber (or frequency), this function has a maximum value of 1. There are striking differences between the spreading functions. Both forms exhibit the previously observed structure where they are narrowest at the spectral peak and broaden both above and below this value. The wavenumber form is clearly bi-modal above the spectral peak. In contrast, however, the frequency form is uni-modal at all frequencies. This difference clearly indicates that a simple transformation between the frequency and wavenumber spectra is not appropriate.

Visual comparison of Fig. 1, panels c and d also shows that, at the spectral peak, the frequency form is broader than the wavenumber form, again signalling that a simple transformation between the spectra is not appropriate.

The directional spreading functions for this case are examined in more detail in Fig. 2, $K(k)$ and Fig. 3, $K(f)$. Fig. 2 shows the directional spreading function, $K(k)$ as a function of direction at values of k/k_p from 0.8 to 8.0. The broadening of the spreading with wavenumber above the spectral peak is clear, as is the bi-modal structure. It is also clear that the bi-modal structure is not symmetric. This was a feature in almost all the observed spreading functions. There was, however, no consistent trend to the asymmetry. For instance, it was not always skewed in one direction.

The frequency form, $K(f)$ in Fig. 3 is shown at values of $\sqrt{f/f_p}$ such that they can be directly compared to the corresponding panel in Fig. 2. This mapping assumes an approximate dispersion relationship of the form $f^2 \propto k$. Therefore, $k/k_p = 4$ can be compared to $\sqrt{f/f_p} = 4$, as an example. The uni-modal structure is clear, in strong contrast to the bi-modal spreading of the wavenumber form. The broader spreading of the frequency form near the energy-containing spectral peak is also clear.

The trends shown for this case (c061323.oc8) hold for all of the spectra under analysis. The frequency spectrum is consistently uni-modal at all frequencies and the wavenumber spectrum uni-modal near the peak and bi-modal at higher wave numbers. As an example of this consistent structure, Fig. 4 shows four typical examples of the directional spreading function $K(k)$ for the wavenumber spectrum. The four cases are shown at $k/k_p = 6$. All clearly show the bi-modal structure seen in Fig. 2.

6. Data analysis and parametric representation

Noting that the wavenumber directional spreading factor does not conform to a common parametric form (e.g. $\cos^2$ or sech^2), the shape independent measure of spreading proposed by Babanin and Soloviev (1998)

$$A^{-1}(k) = \int_0^{2\pi} K(k, \theta) d\theta \tag{14}$$

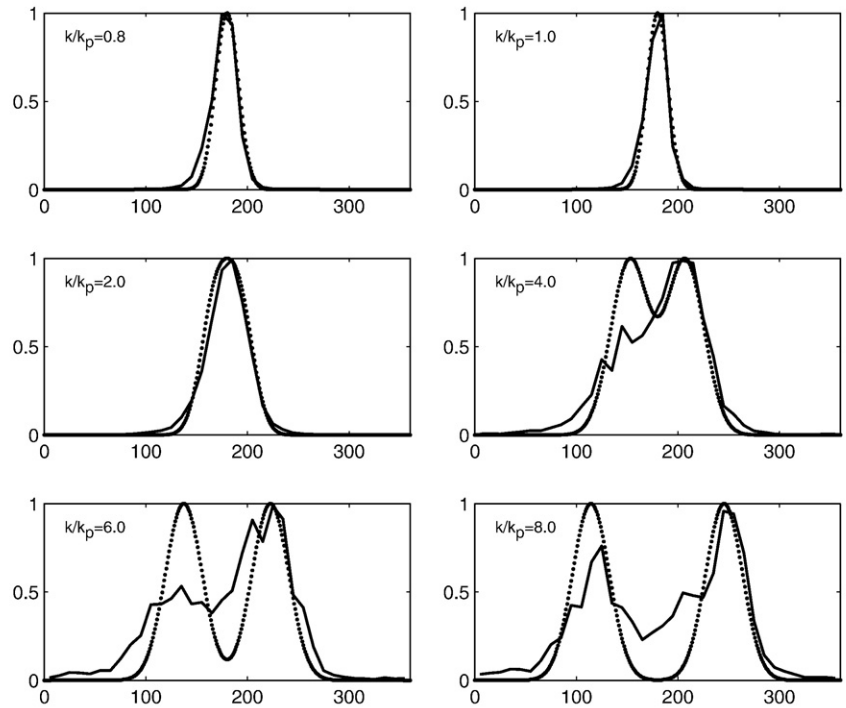

Fig. 2. Slices through the directional spreading function, $K(k, \theta)$ (solid line) at various values of k/k_p (shown on each panel) as a function of direction. The case shown is c061323,oc8 (see Part II). The dotted line is the parametric model defined by Eqs. (17), (18) and (19).

was applied to the full data set. Fig. 5 shows both $A(k)$ and $A(f)$ as functions of k/k_p and f/f_p, respectively. Noting that a large value of A represents narrow spreading, Fig. 5 confirms that both spectra are narrowest at the spectral peak and increase in width for wavenumbers (frequencies) above and below the peak.

Fig. 5 also confirms that the directional wavenumber spectrum is narrower at the peak than the directional frequency spectrum. Values of $A(k_p) \approx 2$ compare with $A(f_p) \approx 1.6$. As the directional spreading is uni-modal at the peak, it is possible to compare these values of A with previously reported values of $\cos^{2s} \theta/2$ distributions. A value of $A \approx 2$ corresponds to $s \approx 50$ and $A \approx 1.6$ corresponds to $s \approx 35$. These results indicate that the present data, or the analysis technique, yield spectra significantly narrower than previously reported. Mitsuyasu et al. (1975), Hasselmann et al. (1980) and Young et al. (1996) all report values of the directional frequency spectrum with $s_p \approx 11$, where s_p represents the value of s at the spectral peak. The Donelan et al. (1985) results, when converted to an equivalent s value reveal $s_p \approx 25$. These differences are discussed further in Section 7.

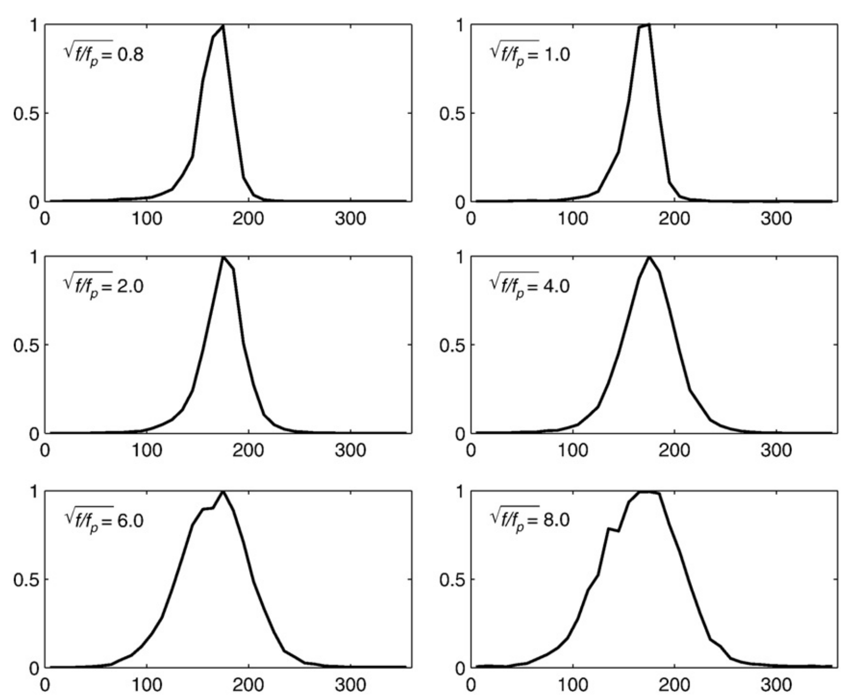

Fig. 3. Slices through the directional spreading function, $K(f, \theta)$ at various values of f/f_p as a function of direction. The values are shown as $\sqrt{f/f_p}$, such that each panel can be directly compared to the corresponding panel of Fig. 2. The case shown is c061323,oc8 (see Part II).

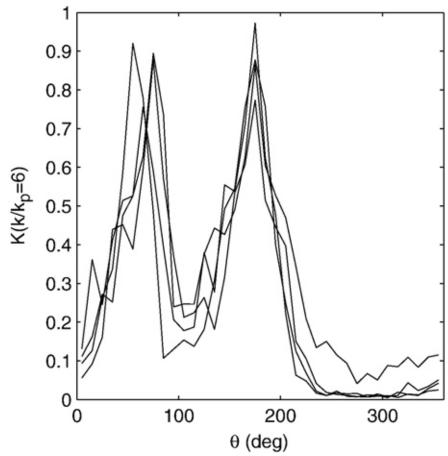

Fig. 4. Four examples of the directional spreading function $K(k, \theta)$ from the data set. In each case, the function is shown for $k/k_p = 6$.

A least-squares fit to the data yields the following parametric representation of the values of A

$$A(k) = \begin{cases} 2.393(k/k_p)^{0.725} & \text{for}\, k/k_p < 0.934 \\ 2.133(k/k_p)^{-0.955} & \text{for}\, 0.934 < k/k_p < 3.6 \\ 0.63 & \text{for}\, k/k_p \ \ 3.6 \end{cases} \tag{15}$$

$$A(f) = \begin{cases} 2.088(f/f_p)^{1.7} & \text{for}\, f/f_p < 0.917 \\ 1.634(f/f_p)^{-1.115} & \text{for}\, f/f_p \ \ 0.917 \end{cases} \tag{16}$$

As a first approximation to the bi-modal structure of the directional wavenumber spectrum, the following parameterisation was investigated

$$K(k) = \cos^{2s(k)}\left(\frac{\theta - \Delta\theta(k)/2}{2}\right) + \cos^{2s(k)}\left(\frac{\theta + \Delta\theta(k)/2}{2}\right) \tag{17}$$

Eq. (17) has two symmetric lobes, separated by $\Delta\theta(k)$ (i.e. $\pm\Delta\theta(k)/2$). In order to apply Eq. (17) it is necessary to estimate the two parameters, $s(k)$ and $\Delta\theta(k)$, both being functions of k (or k/k_p).

All spectra in the full data set were examined and the positions of the lobe maxima and the magnitude of the "trough" between the maxima determined. Fig. 6 shows the mean values of $\Delta\theta$ as a function of k/k_p. Also shown is the ratio of the maximum value of K to the value of the "trough" between the maxima (e.g. a ratio of 0.5 indicates that the trough is half the magnitude of the lobe).

The values of $\Delta\theta$ follow an approximately linear relationship, as a function of k/k_p, and can be approximated by the relationship

$$\Delta\theta(k) = 15.3(k/k_p) - 6.5 \tag{18}$$

where $\Delta\theta$ has units of degrees. As is clear in Fig. 2, the separation of the lobes increases with increasing k/k_p. The value of the lobe ratio decreases with k/k_p, consistent with a model of the form represented by Eq. (17).

The width of the spreading has already been investigated in terms of the parameter A in Fig. 5 and Eq. (15). In order to determine the corresponding values of s, Eq. (17) was numerically integrated for a range of values of s and the resulting values of A recorded. The resulting relationship between s and k/k_p is shown in Fig. 7.

These results were approximated by

$$s(k) = \begin{cases} 71.45(k/k_p)^{1.481} & \text{for}\, k/k_p < 0.934 \\ 61.04(k/k_p)^{-0.85} & \text{for}\, 0.934 < k/k_p < 3.7 \\ 20.0 & \text{for}\, k/k_p \ \ 3.7 \end{cases} \tag{19}$$

Eqs. (17)–(19) define the parametric approximation to $K(k)$. This result is compared with the recorded case in Fig. 2. It represents a reasonable approximation to the directional spreading, noting the asymmetry in this recorded case. The parametric form appears to overestimate the depth of the "trough" between the bi-modal lobes.

The relationships (17)–(19) have been developed for spectra which are at the asymptotic depth limit $\varepsilon_d = 1.0 \times 10^{-3}\delta^{1.2}$ where $\varepsilon_d = g^2 E_{Tot}/U_{10}^4$, $\delta = gd/U_{10}$ and E_{Tot} is the total energy of the wave field (i.e. the significant wave height, $H_s = 4\sqrt{E_{Tot}}$) (see Part I). However, these relationships seem to also apply to spectra within the data set which have not reached this limit. Therefore, it appears that these parameterizations are a reasonable approximation for transitional depth waters such that $0.71 < k_p d < 3.5$. As noted in Part I, wind generated waves (as opposed to swell) do not occur for values of $k_p d < 0.7$.

The results are applicable for the wavenumber range $k_p < k < 10k_p$. The high wavenumber $k \approx 10k_p$ represents the limit of the resolving power of the wave gauge array used and no attempt has been made to parameterize the spectrum in detail below the wavenumber peak.

7. Discussion of results

The results presented above raise a number of interesting questions, which need to be considered. The first of these is how is

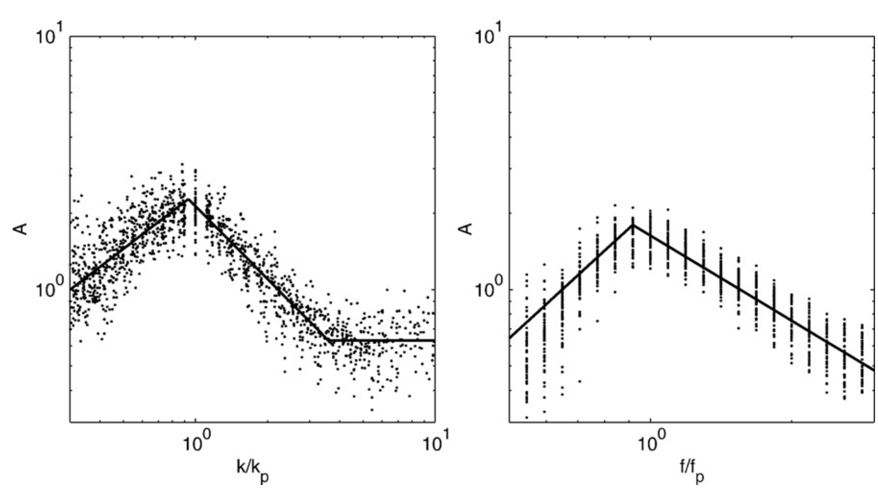

Fig. 5. The directional width parameter $A(k)$ (left panel) and $A(f)$ (right panel), as defined by Eq. (14). Results for all cases in the full data set are shown. The solid lines represent the parametric fits to the data. Eq. (15) is shown in the left panel and Eq. (16) in the right panel.

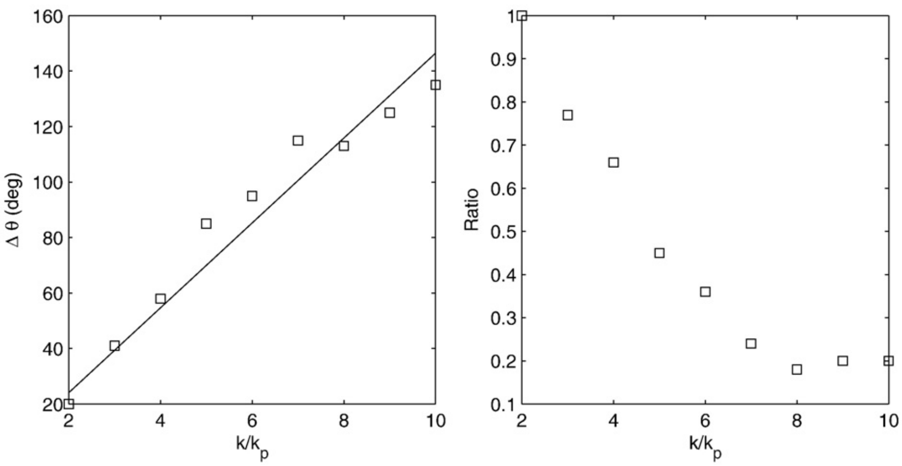

Fig. 6. The mean values of $\Delta\theta$ for the full data set as a function of k/k_p (left panel) and the ratio of the maximum value of K to the value of the "trough" between the maxima (e.g. a ratio of 0.5 indicates that the trough is half the magnitude of the lobe) (right panel). The solid line in the left panel is the relationship (18).

it possible for the directional wavenumber spectrum to be bi-modal, whilst the directional frequency spectrum is uni-modal? Clearly, if there is a linear dispersion relationship relating wavenumber and frequency, the shapes of the spreading should be similar. If, however, some process results in a more complex mapping between wavenumber and frequency, then it is possible for the directional spreading of the two forms to differ.

Fig. 8 shows the same case considered earlier (c061323.oc8). Slices through both wavenumber and frequency spectra are shown at angles of 0°, 20°, 40°, 60°, and 80° respectively. Examination of these spectra shows that if the slices of the wavenumber spectrum at 0° and 20° were displaced to higher values of wavenumber (i.e. displaced to the right), then a form consistent with the frequency spectrum shown in the figure would result. That is, a more complex mapping between wavenumber and frequency could account for the differences in directional spreading between wavenumber and frequency spectra.

The WDM provides a direct means to investigate the relationship between wavenumber and frequency, through the directional wavenumber–frequency spectrum, $\Psi(k, f, \theta)$. Fig. 9 shows $\Psi(k, f, \theta)$ at 0°, 20°, 40°, and 60°. The values of Ψ shown in Fig. 9 have been multiplied by $k^{2.5}$, so as to elevate the tail and normalized such that the maximum value is 1. Contours have been drawn from 1 to 0.005. The vertical dashed line shows the value of k_p and the horizontal dashed line the value of f_p. The linear dispersion relationship, $\omega^2 = gk \tanh kd$, is shown by the dotted line. The energy at each of the angles lies close to the dispersion line. At $\theta = 0°$, the spectral peak aligns well with the dispersion relationship. With increasing wavenumber (frequency), the energy increasingly deviates from the linear dispersion relationship, with the energy being shifted to higher frequencies. Such a result is consistent with energy in the frequency spectrum being displaced to higher frequencies (i.e. moved to the right). A similar result occurs at $\theta = 20°$. At $\theta = 40°$, 60°, however, the situation starts to change. There is now little energy near the spectral peak and the high frequency components are more closely aligned with the dispersion line.

The impact of energy deviating from the dispersion shell in this manner is shown diagrammatically in Fig. 10. The solid line in this figure represents the high frequency face of the frequency spectrum assuming a linear dispersion relationship with the wavenumber spectrum. If, however, wavenumbers map to higher frequencies, as indicated at $\theta = 0°$, 20°, then the spectral energy is displaced to the right, effectively elevating the spectral levels.

As shown in Fig. 9, this process does not occur at larger angles, hence the elevation of the spectral tail of the frequency spectrum is a maximum in the wind direction and decreases with increasing angles to the wind. Such a model is consistent with the observed differences between the wavenumber and frequency spectra. The wavenumber spreading is bi-modal with the maximum energy occurring at an angle to the mean wind direction. In the frequency spectrum, however, the wind direction energy is displaced to higher frequencies, elevating the energy in the wind direction and resulting in the observed uni-modal spreading.

The recorded data cannot directly determine the mechanism responsible for this observed relationship between wavenumber and frequency. However, it is possible to investigate processes which may be consistent with the observed results. One of the major differences between wavenumber and frequency spectra is that frequency spectra are subject to Doppler shifting. At $f/f_p = 3$, the waves are "riding" on energetic waves near the peak of spectrum with wavelengths 10 times longer than the components under consideration. Banner (1990) has shown that the Doppler shifting caused by such effects can be considerable and tend to elevate the energy in the spectral tail. The Banner (1990) result used a two-scale approximation to the continuous spectrum. Effectively, the Doppler shifting will cause the spectral tail to "displace" to higher frequencies. This effect increases with frequency and also with the energy of the dominant waves. It should be noted, however, that the Banner result was for higher frequencies than noted here and that little Doppler shifting was predicted below $f/f_p = 3$.

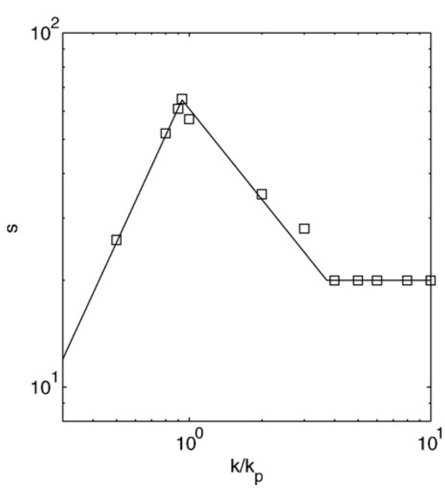

Fig. 7. Mean values of the width parameter s for the full data set as a function of k/k_p. The piecewise solid line is the relationship (19).

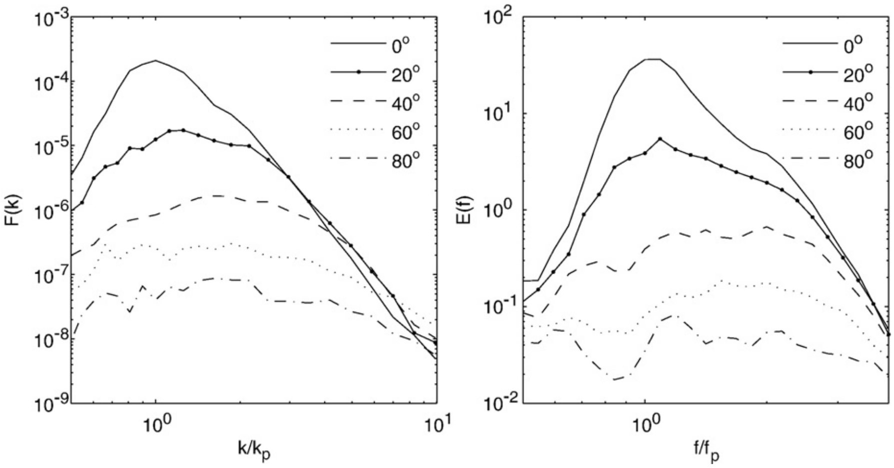

Fig. 8. Slices through the directional wavenumber spectrum (left panel) and directional frequency spectrum (right panel) at various angles to the mean direction. Slices are shown at 0, 20, 40, 60 and 80° to the mean.

As shown in Figs. 1 and 5, the dominant waves near the spectral peak have a narrow directional spread. These waves might cause Doppler shifting of waves in this same direction in the spectral tail. At greater angles to this dominant direction, however, the energy in the dominant waves decreases quickly (more quickly than in the tail). Therefore, at greater angle to the mean direction, it could be expected that the effects of Doppler shifting would decrease. As a result, Doppler shifting might elevate spectral levels in the dominant wind direction but have a smaller effect at greater angles to the wind direction. Therefore, if the wavenumber spectrum is bi-modal, Doppler shifting could elevate the energy levels in the “trough” region between the lobes, but have little impact at greater angles. The result would be a frequency spectrum with reduced bi-modality or possibly a uni-modal structure, as it appears in the present data. Of course, for this mechanism to be significant, Doppler influences would need to occur below $f/f_p = 3$, which is yet to be demonstrated and is beyond the scope of this study.

It is also possible that a combination of nonlinear effects and Doppler shifting simply smears the high frequency tail energy thus masking any bi-modal signature in the frequency spectrum.

The reason why the frequency spectrum is broader at the peak than the wavenumber spectrum is less clearly apparent. However, as can be seen in Fig. 9, at angles greater than 20°, energy remains in the spectrum at $f \leq f_p$. The same is not the case for wavenumber, where there is a much sharper cut-off. The reason for this behaviour is most likely due to nonlinear effects of the finite-depth conditions. It has already been shown that the harmonic at $2f_p$ is a result of triad-type interactions (i.e. $f_p + f_p = 2f_p$). Difference interactions in the spectral tail will potentially result in some energy appearing at f_p. For instance, the difference interaction $3f_p - 2f_p = f_p$, will result in energy

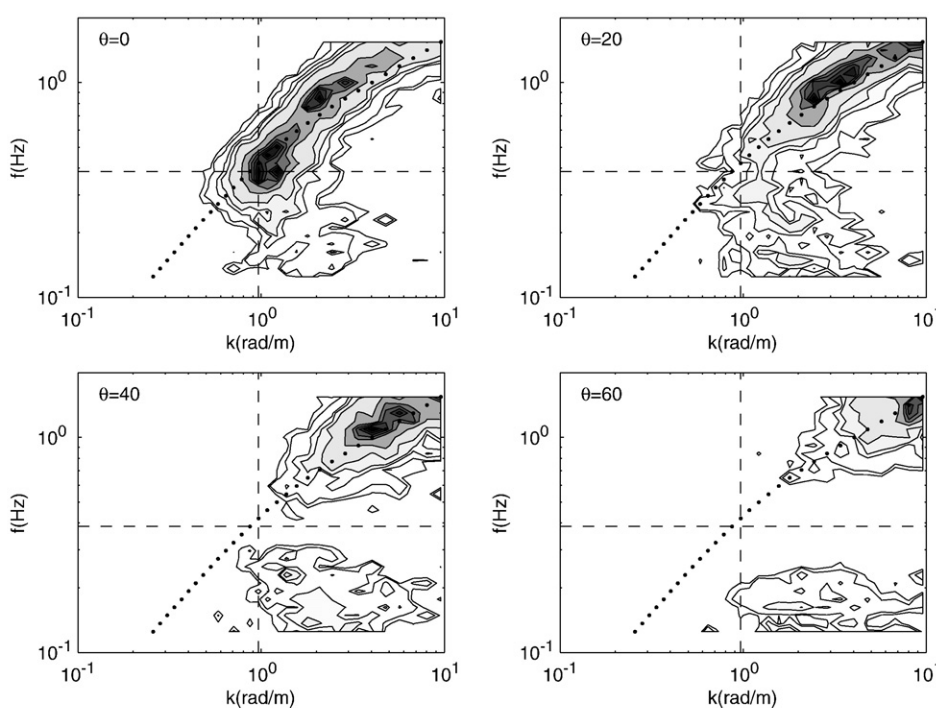

Fig. 9. The wavenumber–frequency–direction spectrum, $\Psi(k, f, \theta)$ at angles of 0°, 20°, 40°, and 60°. The values of Ψ have been multiplied by $k^{2.5}$, so as to elevate the tail and normalized such that the maximum value is 1. Contours have been drawn from 1 to 0.005. The vertical dashed line shows the value of k_p and the horizontal dashed line the value of f_p. The linear dispersion relationship, $\omega^2 = gk\tanh kd$, is shown by the dotted line. The case shown is c061323.oc8 (see Part II).

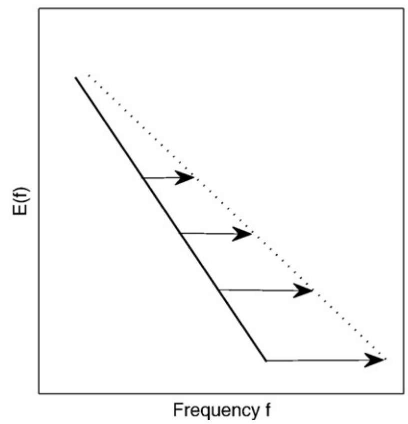

Fig. 10. Diagram showing the high frequency face of the frequency spectrum, assuming a linear dispersion relationship (solid line). If the dispersion relationship does not hold and wavenumbers map to frequencies higher than predicted by the linear dispersion relationship, the spectrum will be displaced to the right (higher frequencies) (dotted line). As a result, deviation from the dispersion relationship can elevate the energy level of the frequency spectrum.

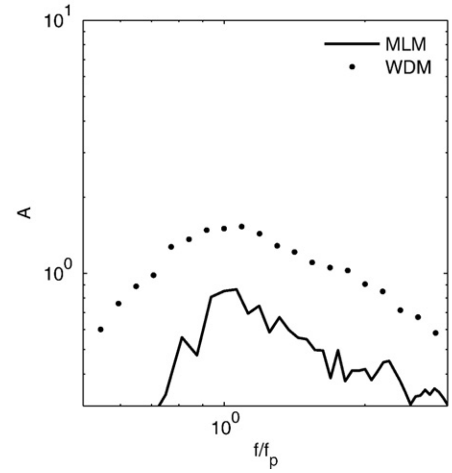

Fig. 11. The directional width parameter $A(f)$ determined from the Maximum Likelihood Method (MLM) (solid line). Also shown are values calculated using the Wavelet Directional Method (WDM) (dots). The scale is the same as in Fig. 5 to facilitate a direct comparison. The case shown is c061323.oc8 (see Part II).

appearing near the spectral peak. These types of interactions will smear the energy in the frequency spectrum in both frequency and direction space, potentially resulting in broader spreading at the spectral peak. Whether such a mechanism can account for the magnitude of the differences observed cannot be determined from the data. However, Fig. 9 clearly shows much greater smearing of energy in the frequency spectrum.

Whether one considers the frequency spectrum or the wavenumber spectrum, the present results indicate much narrower spreading near the peak than has previously been recorded. The present analysis indicates that, for the wave number spectrum, at the spectral peak, $A_p \approx 2$corresponding to $s_p \approx 50$ and for the frequency spectrum, $A_p \approx 1.6$ corresponding to $s_p \approx 35$. All previous measurements [Mitsuyasu et al. (1975), Hasselmann et al. (1980) , Donelan et al. (1985), Young et al. (1996), Babanin and Soloviev, 1998] report values of the directional frequency spectrum with $s_p \approx 10$–25 (or $A_p \approx 0.95$–1.3), where s_p represents the value of s at the spectral peak. These previous results cover both deep and intermediate-depth water. In fact, the results of Young et al. (1996) are from Lake George, as for the present data set. Therefore, the differences cannot be explained by finite-depth influences. The other major difference is the analysis technique. The previous results used a variety of Fourier and MLM methods, whereas the present results use the WDM.

In order to investigate the influence of the analysis technique, the present data was re-analysed using the Maximum Likelihood Method (MLM). Fig. 11 shows values of the parameter $A(f)$ evaluated using the MLM. The maximum value, $A_p \approx 0.9$ is consistent with previous analyses. Also shown in Fig. 11 is the result for the present WDM analysis (for the frequency spectrum). As expected, the values of A are significantly larger than the MLM analysis with $A_p \approx 1.5$, signifying narrower spreading.

It therefore appears that the WDM produces narrower directional spreading than the Fourier techniques. As indicated above, the WDM relies on fewer assumptions in its analysis than the Fourier techniques and therefore one might assume that the results of this analysis may be more reliable. Fortunately, independent comparative studies are available to resolve this issue. Waseda et al. (2008) produced known directional spectra in a directional wave basin and then analysed the wave field using a number of different techniques. They concluded that the WDM was the only method which was able to reproduce the known directional spectrum accurately. Their analysis included techniques such as the MLM.

The differences between the values of A in Fig. 11 are very significant. In order to investigate what such a difference really means in terms of the directional spreading, Fig. 12 shows the directional spreading function $K(f=f_p, \theta)$, derived from the WDM for the same case considered above (i.e. same as shown in Fig. 3, top right panel). For comparative purposes, the spreading functions for Mitsuyasu et al. (1975), Hasselmann et al. (1980) and Donelan et al. (1985) are also shown. As indicated above, the WDM produces results which are narrower than these previous analyses, although the present results are comparable to the high resolution results of Donelan et al. (1985). The differences are, however, not as striking as one might infer from Fig. 11.

Hence, it is reasonable to assume that previous measurements of the directional frequency spectrum were excessively broad as a result of the analysis technique used. This is consistent with the analytical results of Young (1994), which showed that the MLM produced excessively broad results.

Although not shown here, the MLM also produced bi-modal frequency spectra at frequencies above $2f_p$. This is also inconsistent with the WDM analysis and again it is reasonable to assume that the MLM analysis is questionable. Young (1994) pointed out that the MLM has a tendency to create artificial side lobes. The MLM relies on the assumption that the linear dispersion relationship holds. This relationship is used to interpret the cross-spectra between the various gauges. As the present analysis shows, this assumption is questionable at higher frequencies.

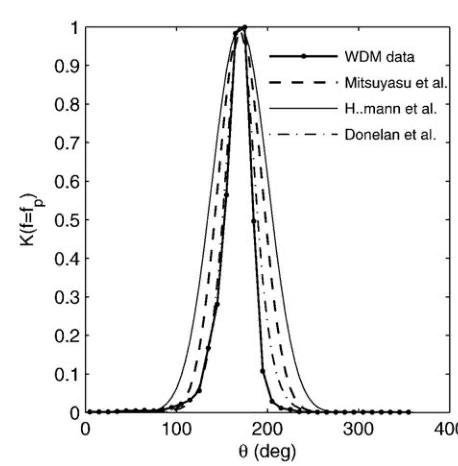

Fig. 12. The directional spreading for the frequency spectrum at $f=f_p$ for case c061323.oc8 derived from the WDM (solid line with dots). For comparative purposes, the analytical functions reported in previous studies are also shown.

As seen in Figs. 2 and 4, the directional spreading is often asymmetric. There was no consistent trend in this asymmetry. For instance, the spectra were not always skewed in one direction. Therefore, it is unlikely that the asymmetry is caused by bathymetry of fetch geometry. It is more likely that such asymmetry is a natural feature of the spectral balance of such high frequency waves (note that at $2f_p$ the waves are typically of frequency 2 Hz). As demonstrated by Young and van Vledder (1993), the high frequency tail of the spectrum is dynamic. The processes of atmospheric input, dissipation and 4-wave nonlinear interaction are in balance in the mean, but imbalances occur on shorter time scales. These imbalances are smoothed by the 4-wave nonlinear interactions, which continually force the spectrum back to the mean state. Therefore, it is likely that the asymmetry observed in the present data (and also present in data analysed using Fourier methods) is a result of these short-term energy imbalances in the spectral tail.

8. Conclusions

The results of this paper have provided a description of the directional spreading of both the wavenumber and frequency spectra of the asymptotic depth-limited wind-wave spectrum. There are significant differences in the spreading of these two forms. The wavenumber spectrum is bi-modal, consistent with previous measurements. In contrast, the frequency spectrum is uni-modal. This apparent conflict is explained by energy in the wind direction at high frequencies being displaced from the linear dispersion shell. This results in an elevation of the spectral tail of the frequency spectrum in the wind direction and hence masks any bi-modality. Although the data cannot define the physical processes responsible for the deviation from the dispersion relationship, it is probable that a combination of Doppler shifting by the dominant waves in the spectrum and nonlinear processes play a role. This is an important finding as it supports previous suggestions that it is the wavenumber spectrum which represents the universal form (e.g. Banner, 1990; Bouws et al., 1985, 1987).

The analysis cannot determine the physical processes responsible for the bi-modal structure of the wavenumber spectrum. However, it is highly likely that 4-wave nonlinear interactions are responsible, as suggested by Banner and Young (1994).

The analysis in this paper clearly shows the power of the Wavelet Directional Method for the analysis of ocean wave time series. The present application is to spatial array data, however, the approach can also be applied to directional wave buoy data. Therefore, it would be possible to routinely obtain wavenumber spectra from such instruments. As the wavenumber spectrum is inherently more robust, as it is not subject to the influences of Doppler shifting, the more extensive use of such wavenumber spectra should be considered in ocean engineering applications.

Combined with Parts I and II, the present paper provides a full description of the depth-limiting form of the wind-wave spectrum. These three papers provide detailed relationships for the asymptotic limits to growth of non-dimensional energy and peak frequency as a function of non-dimensional water depth. In addition, parametric relationships for the one-dimensional frequency and wavenumber spectra are also obtained. Finally, a full parametric description of the directional spreading functions for the wavenumber spectrum is presented. These relationships fully define this important asymptotic limit to grow and allow its routine application in design processes.

Acknowledgements

The authors gratefully acknowledge the financial support of the U.S. Office of Naval Research (grants N00014-97-1-0234, N00014-97-1-0277 and N0014-97-1-0233) and the Australian Research Council (grant A00102965). We also express our gratitude to the staff and students of the School of Civil Engineering of the Australian Defence Force Academy: Jim Baxter, Karl Shaw, Ian Shephard and Michael Wilson who offered highly professional and prompt responses to all urgent demands during the experiments.

References

Alpers, W.R., Ross, D.B., Rufenach, C.L., 1981. On the detectability of ocean surface waves by real and synthetic aperture radar. J. Geophys. Res. 86, 6481–6498.

Babanin, A.V., Soloviev, Y.P., 1998. Variability of directional spectra of wind-generated waves, studied by means of wave staff arrays. Mar. Freshw. Res. 49, 89–101.

Banner, M.L., 1990. Equilibrium spectra of wind waves. J. Phys. Oceanogr. 20, 966–984.

Banner, M.L., Young, I.R., 1994. Modeling spectral dissipation in the evolution of wind waves — part 1. Assessment of existing model performance. J. Phys. Oceanogr. 24, 1550–1671.

Banner, M.L., Jones, I.S.F., Trinder, J.C., 1989. Wavenumber spectra of short gravity waves. J. Geophys. Res. 73, 513–530.

Bottema, M., 2007. Measured wind-wave climatology Lake IJssel (NL), report RWS RIZA 2007.020. 978-90-369-1399-7. 278 pp.

Bottema, M., van Vledder, G.Ph., 2009. A ten-year data set for fetch- and depth-limited wave growth. Coast. Eng. 56, 703–725. doi:10.1016/j.coastaleng.2009.01.012.

Bouws, E., Günther, H., Rosenthal, W., Vincent, C.L., 1985. Similarity of the wind wave spectrum in finite depth water, 1. Spectral form. J. Geophys. Res. 90, 975–986.

Bouws, E., Günther, H., Rosenthal, W., Vincent, C.L., 1987. Similarity of the wind wave spectrum in finite depth water, 2. Statistical relationships between shape and growth stage parameters. Dtsch. Hydrogh. Z. 40, 1–24.

Bretschneider, C.L., 1958. Revisions in wave forecasting: deep and shallow water. Proc. 2nd Conf. on Coastal Eng., ASCE, Council on Wave Research.

Donelan, M.A., Hamilton, J., Hui, W.H., 1985. Directional spectra of wind-generated waves. Philos. Trans. R. Soc. Lond., A 315, 509–562.

Donelan, M.A., Drennan, W.M., Magnusson, A.K., 1996. Nonstationary analysis of the directional properties of propagating waves. J. Phys. Oceanogr. 26, 1901–1914.

Ewans, K.C., 1998. Observations of the directional spectrum of fetch-limited waves. J. Phys. Oceangr. 28, 495–512.

Hasselmann, K., 1962. On the non-linear energy transfer in a gravity-wave spectrum, part 1. General theory. J. Fluid Mech. 12, 481–500.

Hasselmann, D.E., Dunckel, M., Ewing, J.A., 1980. Directional wave spectra observed during JONSWAP 1973. J. Phys. Oceanogr. 10, 1264–1280.

Hasselmann, K., Raney, R.K., Plant, W.J., Alpers, W., Schuchman, R.A., Lyzenga, D.R., Rufenach, C.L., Tucker, M.J., 1985. Theory of synthetic aperture radar ocean imaging — a MARSEN view. J. Geophys. Res. 90, 4659–4686.

Holthuijsen, L.H., 1983. Observations of the directional distribution of ocean-wave energy in fetch-limited conditions. J. Phys. Oceanogr. 13, 191–207.

Hwang, P.A., Wang, D.W., Walsh, E.J., Krabill, W.B., Swift, R.N., 2000. Airborne measurements of the wavenumber spectrum of ocean surface waves. Part II: directional distribution. J. Phys. Oceangr. 30, 2768–2787.

Isobe, M., Kondo, K., Horikawa, K., 1984. Extension of MLM for estimating directional wave spectrum. Symp. on Description and Modelling of Directional Seas, DHI and MMI, Copenhagen, pp. 1–15.

Krogstad, H.E., Magnusson, A.K., Donelan, M.A., 2006. Wavelet and local analysis of ocean waves. Int. J. Offshore Polar Eng. 16 (2), 97–103.

Longuet-Higgins, M.S., Cartwright, D.E., Smith, N.D., 1963. Observations of the directional spectrum of sea waves using the motions of a floating buoy. Ocean Wave Spectra. Prentice Hall, pp. 111–136.

Lygre, A., Krogstad, H.E., 1986. Maximum entropy estimation of the directional distribution in ocean wave spectra. J. Phys. Oceanogr. 16, 2052–2060.

Mitsuyasu, H., Tasai, F., Suhara, T., Mizuno, S., Onkusu, M., Honda, T., Rukiiski, K., 1975. Observations of the directional spectrum of ocean waves using a cloverleaf buoy. J. Phys. Oceanogr. 5, 751–761.

Pierson, W.J., Moskowitz, L., 1964. A proposed spectral form for fully developed wind seas based on the similarity theory of S.A. Kitaigorodskii. J. Geophys. Res. 69, 5181–5190.

Resio, D.T., Long, C.E., Vincent, C.L., 2004. Equilibrium-range constant in wind-generated wave spectra. J. Geophys. Res. 109, C01018. doi:10.1029/2003JC001788.

Thijsse, J.Th., 1949. Dimensions of wind-generated waves. General Assembly of Association d'Ocèanographie Physique, Procès-Verbaux, 4, Oslo, pp. 80–81.

U.S. Army Corps of Engineers, 1955. Waves and wind tides in shallow lakes and reservoirs. Summary Report, Project CW-167, Jacksonville District, Fla.

Walsh, E.J., Hancock III, D.W., Hines, D.E., 1989. An observation of the directional wave spectrum evolution from shoreline to fully developed. J. Phys. Oceanogr. 19, 670–690.

Wang, D.W., Hwang, P.A., 2001. Evolution of the bimodal directional distribution of ocean waves. J. Phys. Oceanogr. 31, 1200–1221.

Waseda, T., Kinoshita, T., Tamura, H., 2008. Evolution of a random directional wave and freak wave occurrence. J. Phys. Oceanogr. 38. doi:10.1175/2008JPO4031.1.

Wyatt, L.R., 1995. The effect of fetch on the directional spectrum of Celtic Sea storm waves. J. Phys. Oceanogr. 25, 1550–1559.

Young, I.R., 1994. On the measurement of directional wave spectra. Appl. Ocean Res. 16, 283–294.

Young, I.R., van Vledder, G.Ph., 1993. A review of the central role of nonlinear interactions in wind-wave evolution. Philos. Trans. R. Soc. Lond., A 342, 505–524.

Young, I.R., Verhagen, L.A., 1996a. The growth of fetch limited waves in water of finite depth. Part I: total energy and peak frequency. Coast. Eng. 28, 47–78.

Young, I.R., Verhagen, L.A., 1996b. The growth of fetch limited waves in water of finite depth. Part II: spectral evolution. Coast. Eng. 28, 79–100.

Young, I.R., Babanin, A.V., 2006. The form of the asymptotic depth-limited wind-wave frequency spectrum. J. Geophys. Res. 111, C06031. doi:10.1029/2005JC003398.

Young, I.R., Babanin, A.V., 2009. The form of the asymptotic depth-limited wind-wave spectrum: part II — the wavenumber spectrum. Coast. Eng. 56, 534–542. doi:10.1016/j.coastaleng.2008.11.005.
Young, I.R., Rosenthal, W., Ziemer, F., 1985. A three-dimensional analysis of marine radar images for the determination of ocean wave directionality and surface currents. J. Geophys. Res. 90 (C1), 1049–1060.
Young, I.R., Verhagen, L.A., Banner, M.L., 1995. A note on the bi-modal directional spreading of fetch-limited wind waves. J. Geophys. Res. 100 (C1), 773–778.
Young, I.R., Verhagen, L.A., Khatri, S.K., 1996. The growth of fetch limited waves in water of finite depth. Part III: directional spectra. Coast. Eng. 28, 101–122.
Young, I.R., Banner, M.L., Donelan, M.A., Babanin, A.V., Melville, W.K., Veron, F., McCormick, C., 2005. An integrated system for the study of wind-wave source terms in finite-depth water. J. Atmos. Ocean. Technol. 22 (7), 814–831.